

Enhanced molybdenum(VI) adsorption by zirconia sol-modified nanoscale iron sulfide: performance, mechanism and influencing factors

Jian-jun Lian^a, Meng Wu^a, Hong-yan Wu^a, Yan-ting Liu^a, Qing Xu^a, Man-jun Miao^a, Jian-hua Yang^a, Ke-ke Mao^{a,*}, Bo Chen^a, Feng Xue^{b,*}, Qiao-ping Kong^c, Ming-hao Shang^a, Xiu-ling Li^d

^aCollege of Energy and Environment, Anhui University of Technology, Anhui 243002, China, emails: jjlian85@126.com (J.-j. Lian), 1723834029@qq.com (M. Wu), 2414195879@qq.com (H.-y. Wu), 1085254512@qq.com (Y.-t. Liu), 1319987478@qq.com (Q. Xu), 2251678731@qq.com (M.-j. Miao), 316034129@qq.com (J.-h. Yang), maokeke@ahut.edu.cn (K.-k. Mao), greenchenbo@163.com (B. Chen), 2810794642@qq.com (M.-h. Shang)

^bNanjing Institute of Environmental Sciences, Ministry of Ecology and Environment, Nanjing, Jiangsu 210042, China, email: fuxinet@126.com (F. Xue)

^cSchool of Environmental and Municipal Engineering, Qingdao University of Technology, Qingdao, Shandong 266033, China, email: kongqiaoping@qut.edu.cn (Q.-p. Kong)

^dSchool of Physical Science and Technology, Nanjing Normal University, Nanjing 210023, China, email: xlli@njnu.edu.cn (X.-l. Li)

Received 17 March 2023; Accepted 15 June 2023

ABSTRACT

The significant increase in demand for molybdenum (Mo) resources has led to excessive molybdate (Mo(VI)) content in water, posing a challenge to the innovation of Mo(VI) removal technology in water bodies. Nanoscale iron sulfide (FeS) has an important effect on the environmental behavior of Mo(VI) in aquatic solutions. To address the issue of easy agglomeration and poor stability of FeS, zirconia sol-modified nanoscale iron sulfide (Zr-FeS) was synthesized, and the adsorption behavior of Zr-FeS on Mo(VI) from diverse aquatic solutions was also investigated in this study. The results showed that the removal rate of Mo(VI) was increased from 28.60% to 78.32% within pH value of 7.0 when Zr/Fe molar ratio was elevated from 0 to 0.5. Moreover, the Mo(VI) adsorption efficiency by Zr-FeS was closely related to pH values, and acid conditions were beneficial for Mo(VI) adsorption. The pseudo-second-order model demonstrated a better fit to the data compared to other models. The maximum adsorption capacity of Zr-FeS towards Mo(VI) value calculated by Langmuir isotherm model was 118.48 mg/g at 298 K. The thermodynamic analysis revealed that the adsorption process of Mo(VI) was endothermic, entropically favorable, and spontaneous in nature. Competing anions (e.g., PO_4^{3-} , HCO_3^- , and SO_4^{2-}) partially inhibited the adsorption process of Mo(VI) by Zr-FeS. While the process was less affected by dissolved oxygen and aging. The results of Fourier-transform infrared spectroscopy, X-ray diffraction, X-ray photoelectron spectroscopy, and density functional theory (DFT) calculations revealed that the main mechanisms for Mo(VI) removal were hydrogen bonding, electrostatic interaction and surface complexation. The high stability and fast adsorption rate indicated that Zr-FeS was a promising material to remove Mo(VI) from the aquatic solutions.

Keywords: Mo(VI) removal; Iron sulfide; Zirconia sol; Adsorption; Density functional theory (DFT) calculation

* Corresponding authors.

1. Introduction

Molybdenum (Mo), an important strategic resource and essential element for organisms, is being mined more and more, which leads to increasing pollution pressure on surface water [1]. The concentration of Mo in surface waters generally is less than 5 µg/L [2]. Excessive accumulation of Mo in the human body can hinder its normal metabolism, leading to bone enlargement, connective tissue degeneration, and developmental retardation [3,4]. However, the massive development of Mo ore has led to serious excesses of Mo in some untreated mining tailwaters, and Mo pollution has become a common problem around the world, that is, Yerevan of the Republic of Armenia and Luanchuan County in China (Table S1). Mo is found in many oxidation states, with a range of -2 to +6 [8]. Specially, hexavalent molybdenum (MoO₄²⁻) has been studied intensively due to its stability and extremely high toxicity.

At present, the treatment technology of Mo-containing wastewater at home and abroad mainly includes chemical precipitation [9], adsorption, ion exchange [10], and membrane separation [11]. The adsorption method is universally adopted in the sewage treatment process due to its economy, efficiency, and ease of operation. So far, several adsorbents have been reported for Mo(VI) removal. Tu et al. have successfully prepared ZnFe₂O₄ and the Mo's maximum adsorption capacity could be reached to 62.5 mg/g [12]. The adsorption of Mo in wastewater by NaOCl-oxidized multiwalled carbon nanotubes was only 22.73 mg/g [13]. Verbinen et al. [14] have studied the simultaneously removal performance of Mo, selenium, and antimony oxyanions from sewage by loading magnetite, and the adsorption capacity of Mo in acidic condition was only 18.02 mg/g. Although the above adsorbents have properties of simple preparation and strong stability, their adsorption rate are relatively low and the adsorption amount is relatively low. Therefore, the primary goal of this study is to find an ideal adsorbent with high stability and high adsorption capacity.

Previous studies have shown that reducing sulfur species such as HS⁻, S²⁻, and S_n²⁻ will effect the migration of Mo. On one hand, sulfur will replace oxygen in Mo^{VI}O₄²⁻, thus changing the migration characteristics of MoO₄²⁻ [15]; On the other hand, sulfur and ubiquitous iron are easy to form iron sulfide minerals, which is easier to capture Mo [16]. Iron monosulfide (FeS) is a non-toxic mineral which is widely existed in the natural environment [17]. Its strong reduction characteristics are crucial for immobilizing some heavy metals like Hg(II) and Se(IV) in reducing environments [18,19]. Our previous researches have proven that FeS had a better removal effect on MoO₄²⁻ in the anaerobic environment [16]. However, the synthetic FeS is usually deactivated by agglomeration and oxidation [Eq. (1)], and is prone to decomposition in acid solution [Eq. (2)].



Zirconia is a kind of inert inorganic oxide. The sol prepared by zirconia has excellent properties such as high temperature resistance, corrosion resistance, abrasion resistance,

and oxidation resistance. Besides, zirconia sol usually has strong ionic affinity due to its large number of hydroxyl groups which can coordinate with oxygen-containing groups [20]. Therefore, zirconia sol-based adsorbent may have good adsorption capacity for nitrate and other anions [21]. For example, ZrO₂ can significantly enhance the adsorption capacity of adsorbents such as metal oxides and activated carbon on heavy metals, which can inhibit the agglomeration of metal oxides, so it is a potential candidate for modification of FeS [22,23]. However, the optimization of the modification parameters of zirconia sol on FeS is not clear. Detailed investigations are still needed on the removal performance, mechanism, and influencing factors of zirconia sol-modified nanoscale iron sulfide (Zr-FeS) on Mo(VI).

In the present work, a novel stable and efficient Zr-FeS was synthesized and the mechanism as well as key factors for Mo(VI) removal were explored. The detailed objectives of this work were: (1) to determine the most suitable parameters for the synthesis of Zr-FeS; (2) to explore Mo(VI) adsorption properties and influencing factors by Zr-FeS; (3) to discern the removal mechanism of Mo(VI) by Zr-FeS via X-ray photoelectron spectroscopy (XPS) and density functional theory (DFT) studies. This work enriches the application of FeS, providing a reference for the removal of Mo(VI) in aquatic solutions.

2. Materials and methods

2.1. Chemical agents

Sodium sulfide (Na₂S·9H₂O) was purchased from Aladdin Reagent Co., Ltd., (Shanghai, China). Na₂MoO₄·2H₂O was used to prepare 1,000 mg/L stock solutions. Ferrous chloride tetrahydrate (FeCl₂·4H₂O) was provided by A Johnson Matthey Company (JM, USA). Zirconium oxychloride octahydrate (ZrOCl₂·8H₂O), potassium nitrate (KNO₃), ethanol (C₂H₅OH), sodium hydroxide (NaOH), sodium dihydrogen phosphate dihydrate (NaH₂PO₄·2H₂O), hydrochloric acid (HCl), sodium sulfate (Na₂SO₄), sodium hydrogen carbonate (NaHCO₃), and sodium molybdate 2-hydrate (Na₂MoO₄·2H₂O) were all purchased from Sinopharm Chemical Reagent Co., Ltd., China. Analytically graded reagents and deionized water were used in all experiments.

2.2. Preparation of Zr-FeS

The Zr-FeS was prepared by mixing FeCl₂·4H₂O, ZrOCl₂·8H₂O, and Na₂S·9H₂O in a 250 mL flask reactor full of N₂ (99.99%) (Wu et al. [24]). Briefly, a certain amount of ZrOCl₂·8H₂O (0.154 mol/L) was dissolved in a 5:3 (v/v) mixture of ethanol and water, and sealed it in a water bath at 70°C for 2 h to prepare zirconia sol. Afterwards, zirconia sol was slowly added into 50 mL of FeCl₂·4H₂O solution (0.2 mol/L) in electric stirring (300 rpm). After 15 min of reaction, 50 mL of Na₂S·9H₂O with the same concentration was supplemented to the above solution, and continued stirring for half an hour to obtain Zr-FeS material. The prepared black nanoparticles were rinsed with deionized water aerated with N₂ for several times and then stored in the ethanol solution. Zr-FeS with different compositions were synthesized by adjusting the addition ratio of the zirconia sol, that is, molar ratios of Zr/Fe (0.1, 0.3, 0.5, 0.8, and 1.0).

Likewise, bare FeS was obtained without adding zirconia sol in the above preparation process.

2.3. Mo(VI) adsorption batch experiments

A series of Zr-FeS suspensions (Zr/Fe = 0.5) were prepared to react with 5–50 mg/L of Mo(VI) vs. dosage (20–200 mg/L) at 180 rpm unless specified otherwise. 0.1 mol/L of KNO₃ was employed to adjust the ionic strength of the solution. 5 mL syringe was utilized to collect samples periodically. After filtering through a filter with a 0.45 μm aperture, the samples were immediately analyzed. Batch experiments were performed to investigate the influences of Zr/Fe molar ratio (0.1, 0.3, 0.5, 0.8, and 1.0), pH (5–9), the dosage of Zr-FeS, and the initial Mo(VI) concentration on Mo(VI) removal. Besides, the Zr/Fe, temperature, pH, Zr-FeS dosage, and Mo(VI) concentration were set at 0.5, 298 K, 7.0, 100, and 10 mg/L as control conditions. 1 mol/L HCl/NaOH was utilized for adjusting the initial pH of the solutions. The influences of competing anions (PO₄³⁻, HCO₃⁻, and SO₄²⁻; used as their 0.1–10 mg/L sodium salts, respectively) and dissolved oxygen (DO) on the removal of Mo were also studied. The nitrogen or oxygen environment in the solution was prepared by continuously injecting nitrogen or pure oxygen into the Mo(VI) solutions for half an hour. In addition, the chemical stability of FeS and Zr-FeS was also analyzed after aging for 0, 7, and 30 d, respectively.

2.4. Regeneration

To evaluate the regenerative ability of Zr-FeS, the adsorption and desorption process of Mo(VI) were studied for consecutive five cycles. In each cycle, 5.0 g/L Zr-FeS were added to 30 mg/L of Mo(VI) solution and the mixture was shaken in a shaker with the speed of 180 rpm for 8 h. After that, the Mo(VI)-adsorbed Zr-FeS were separated by centrifugation and added to the 60 mL of 0.1 mol/L NaOH solution and shaken for 1 h. Then the Zr-FeS were collected after desorption, and the amount of Mo(VI) desorption in the aqueous solution was detected. After each regeneration experiment, Zr-FeS were collected, washed, and dried overnight for the next cycle.

2.5. Analysis

The suspension after reaction equilibrium was subjected to centrifugation for 10 min with 10,000 rpm, and the used adsorbent was dried and stored under nitrogen, and then employed for further analysis of surface morphology and structural changes. The details of analytical methods are provided in Test S1 of Supplementary Information.

2.6. Theoretical interatomic adsorption analysis by DFT

The Vienna ab-initio simulation package (VASP) was adopted to conduct all DFT calculations [25,26]. The Perdew–Burke–Ernzerhof (PBE) exchange–correlation function of the generalized gradient approximation (GGA) was utilized [27], along with the projected enhanced wave (PAW) pseudopotential [28,29], to describe ion nuclei and valence interactions between electrons. After convergence

tests for energy cutoff and k-points, 450 eV was set as the cutoff value. The Monkhorst–Pack scheme was used to sample the Brillouin zone [30], and a 3 × 3 × 1 k-point grid was employed for geometry optimization. The energy and force converge to 1.0 × 10⁻⁴ eV and -0.002 eV/Å. Eq. (3) was used to calculate the adsorption energy:

$$E_{\text{ads}} = E_{\text{adsorption system}} - E_{\text{surface}} - E_{\text{adsorbate}} \quad (3)$$

where $E_{\text{adsorbate}}$, E_{surface} , and $E_{\text{adsorption system}}$ are the respective total energies of the free adsorbate, Zr-FeS, and Zr-FeS with adsorbate.

In thermodynamics, negative values of adsorption energy indicate that the process is exothermic, while positive ones suggest endothermy. The larger negative adsorption energy denotes a more stable adsorption structure. The binding energy between the Mo atom and Zr-FeS(001) can be examined by calculating the charge density difference ($\Delta\rho$) as:

$$\Delta\rho = \rho_{\text{Mo+A}} - (\rho_{\text{Mo}} + \rho_{\text{A}}) \quad (4)$$

where $\rho_{\text{Mo+A}}$, ρ_{A} , and ρ_{Mo} are the charge densities of Mo-adsorbed Zr-FeS(001) structure, pristine Zr-FeS(001) and isolated Mo atoms, respectively, with Mo atoms and A are in the same positions in the Mo+A system.

3. Results and discussion

3.1. Removal performance of Mo(VI) by modified FeS

The removal efficiency of Mo(VI) was increased from 28.60% to 78.32% at pH value of 7.0, when Zr/Fe was expanded from 0 to 0.5 (Fig. 1a). However, as Zr/Fe continuously rises, the enhancement of Mo(VI) removal efficiency was not significant. Thus, the best Zr-FeS modification condition was selected as 0.5. Besides, the removal rate of Mo(VI) by Zr-FeS was significantly higher than that of FeS under different pH conditions (Fig. 1b). Moreover, Mo(VI) removal rate was gradually dropped with the increasing initial pH of the solution for Zr-FeS, and the removal rate was higher than 90% at pH = 4.0. These phenomenon might be related to the Mo morphology in solution and the surface charge of the adsorbents. According to the speciation and solubility curve of MoO₄²⁻ calculated by VISUAL MINTEQ software (Fig. 1c), MoO₄²⁻ was changed to other forms (MoO₃(H₂O)₃ and HMoO₄) in the pH range of 2.0–4.0, which was more conducive to removing Mo(VI) by electrostatic interaction. Besides, the pH_{pzc} of Zr-FeS (6.25) was higher than that of FeS (5.42) (Fig. 1d), which might be induced by the hydroxyl group's protonation on the Zr surface [31]. However, Zr-FeS also had a certain removal effect on Mo(VI) when the pH_{pzc} was higher than 6.25, so electrostatic adsorption was only one of its removal mechanisms.

3.2. Characteristics

As shown in Fig. 2a, some clustered mineral structure was appeared on the surface of unmodified FeS, which might be owing to the partial oxidation of FeS to Fe(OH)₃ [16]. The synthetic Zr-FeS with flocculent dispersion was

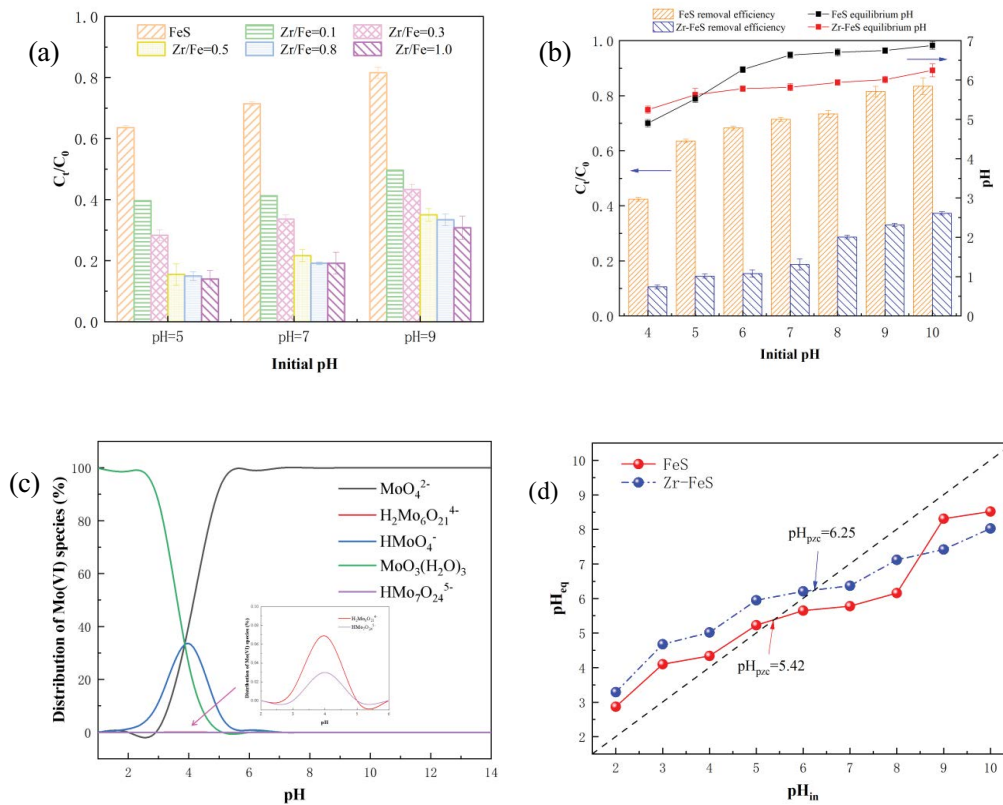


Fig. 1. (a) Mo(VI) removal performance comparison of FeS and Zr-FeS (Zr/Fe = 0.1, 0.3, 0.5, 0.8, 1.0, pH = 5, 7, 9), (b) effect of initial pH on Mo(VI) removal by FeS and Zr-FeS (Zr/Fe = 0.5), (c) distribution of molybdate species as a function of pH at Mo(VI) concentration of 10 mg/L and (d) point of zero charge of FeS and Zr-FeS (Zr/Fe = 0.5).

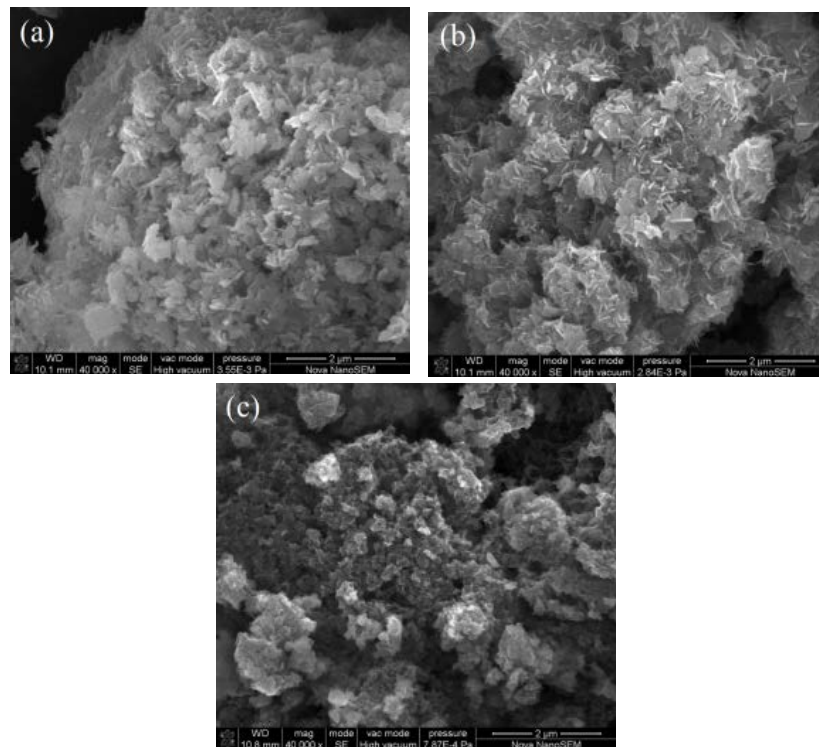


Fig. 2. Scanning electron microscopy images of (a) FeS, (b) Zr-FeS before the reaction with Mo(VI) and (c) Zr-FeS after the reaction with Mo(VI).

full of pores, and the uniformly dispersed flocs might be caused by amorphous hydrated zirconia covered on FeS (Fig. 2b). However, the Zr-FeS surface was transformed into a granular state after reaction with Mo(VI), suggesting that Mo(VI) had been adsorbed on the surface of Zr-FeS and changed its surface morphology (Fig. 2c). Energy-dispersive X-ray spectroscopy (EDS) images (Fig. S1) suggested that Zr-FeS was mainly composed of O, Cl, S, Fe and Zr. After adsorption process, Mo element was appeared on the surface of Zr-FeS. Moreover, the element type in the mapping images (Fig. S2) was also consistent with that shown in the EDS images. The specific surface area of the FeS and Zr-FeS was analyzed by a Brunauer–Emmett–Teller (BET)-N₂ surface area analyzer. The results showed that the Zr-doped FeS had a larger BET surface area (59.92 m²/g) than the FeS (48.67 m²/g). Both FeS nanoparticles and Zr-FeS both exhibited type IV isotherms with an H₃ hysteresis loop, indicating the presence of well-developed mesopores in both materials (Fig. S3) [21,32]. The modification of the FeS by ZrO₂ might cause different surface morphologies and might yield particles with different surface functional groups, thereby affecting the surface area of the particles [33].

3.3. Adsorption kinetics

As shown in Fig. 3a and b, the initial dosage of Zr-FeS and the initial concentration of MoO₄²⁻ dominantly influenced the Mo(VI) removal (pH = 7.0.). Moreover, the rate of removal showed a trend of rapid improvement with the increase of the amount of Zr-FeS and the decreasing initial Mo(VI) concentration. The adsorption active sites was increased as the increase of Zr-FeS dosage increased. Conversely, Mo(VI) with lower concentration was more favorable to be adsorbed by the active sites of Zr-FeS. These findings were consistent with our previous study using FeS to remove Mo(VI) [16]. Since the correlation coefficient $R^2 > 0.98$ and the calculated adsorption amount $q_{e,cal,2}$ was closer to the experimental $q_{e,exp}$ (Table 1 and Fig. 3c–f), the adsorption kinetic process of Mo(VI) by Zr-FeS conformed to the pseudo-second-order kinetic model. Thus, the limiting step of the adsorption rate might be determined by electron sharing or exchange in chemical adsorption [34].

3.4. Adsorption isotherms

Four adsorption models (Freundlich isotherm, Temkin isotherm, Langmuir isotherm, and Dubinin–Radushkevich isotherm) were used to simulate the isothermal adsorption data in this study. As shown in Fig. 4, the Mo(VI) adsorption quickly tended to saturation at three temperatures as the initial Mo(VI) concentration rose. Besides, the Langmuir model with higher correlation coefficient R^2 was superior for fitting the whole adsorption process, and the maximal adsorption capacity (Q_m) was close to the experimental data ($Q_{e,exp}$) (Table 2). Therefore, the Mo(VI) adsorption mainly occurred on the Zr-FeS surface through a single-layer molecular layer adsorption. Compared with some adsorbents (Table 3), Zr-FeS had a higher adsorption capacity for Mo(VI) (118.48 mg/g, 298 K); moreover, the values of dimensionless separation factor (R_L) used to represent a fundamental feature

of the Langmuir isotherm were in 0–1 at various temperatures. These results implied that Zr-FeS has potential application in the treatment of wastewater containing Mo(VI).

3.5. Thermodynamics analysis

Temperature is an important factor in the adsorption process. The Mo(VI) removal process by Zr-FeS under three temperatures (298, 308, and 318 K) were tested in this study. Table 2 illustrates that the Q_m values improved from 118.48 to 205.01 mg/g with elevated temperature, suggesting that increasing the temperature was beneficial to Mo(VI) removal. As shown in Table 4, Mo(VI) adsorption process by Zr-FeS was endothermic, and the randomness was increased at the interface between solid and solution, since the values of enthalpy change (ΔH°) and entropy change (ΔS°) were positive. Besides, the negative Gibbs free energy change (ΔG°) showed that the Mo(VI) adsorption process was spontaneous, and ΔG° values decreased gradually with the increase of temperature, suggesting that high temperature helped the remove of Mo(VI).

3.6. Influencing factors

3.6.1. Influences of competing anions and dissolved oxygen

Anions coexisting with MoO₄²⁻ may preempt the adsorbed material's active site, causing the adsorption effect of the material on Mo(VI) to be weakened. The effects of PO₄³⁻, HCO₃⁻, and SO₄²⁻ on the adsorption performance of Mo(VI) by Zr-FeS were investigated, and the results showed that three oxoacid anions had certain inhibition on Mo(VI) removal, which might be caused by the competition between three oxoacid anions and molybdate for Zr-FeS surface's active adsorption sites (Fig. 5a–c). Therefore, the inhibition was strengthened with the increase in the concentration of oxoacid anions. Additionally, PO₄³⁻ had greater inhibition on removing Mo(VI), which could be caused by the generation of an inner spherical complex between PO₄³⁻ and iron (oxygen) hydroxides [38].

Compared with bare FeS, Mo(VI) adsorption process by Zr-FeS was far less impacted by DO under different DO environments (Fig. 5d). DO significantly inhibits the Mo(VI) adsorption by FeS, which may be caused by the electrons of the ferrous ion are more easily taken up by DO [39]. However, the oxygen-containing layer formed on the FeS surface modified by zirconium sol can not only effectively prevent the erosion of DO, but also has little impact on the transmission of electrons (Zeeshan et al. [40]), thus alleviating the DO influence on removing Mo(VI) by Zr-FeS.

3.6.2. Impact of aging

The aging of nanomaterials usually leads to surface passivation and aggregation of their, which hurts their reducibility. Compared with bare FeS, the aging effect on removing Mo(VI) by Zr-FeS was much lower (Fig. 6a), and the efficiency decreased by 10.39% and 19.40%, respectively after 30 d of aging. FeS was easier to oxidize during the aging process and formed a surface passivation layer. X-ray diffraction (XRD) was further tested to find out the structural

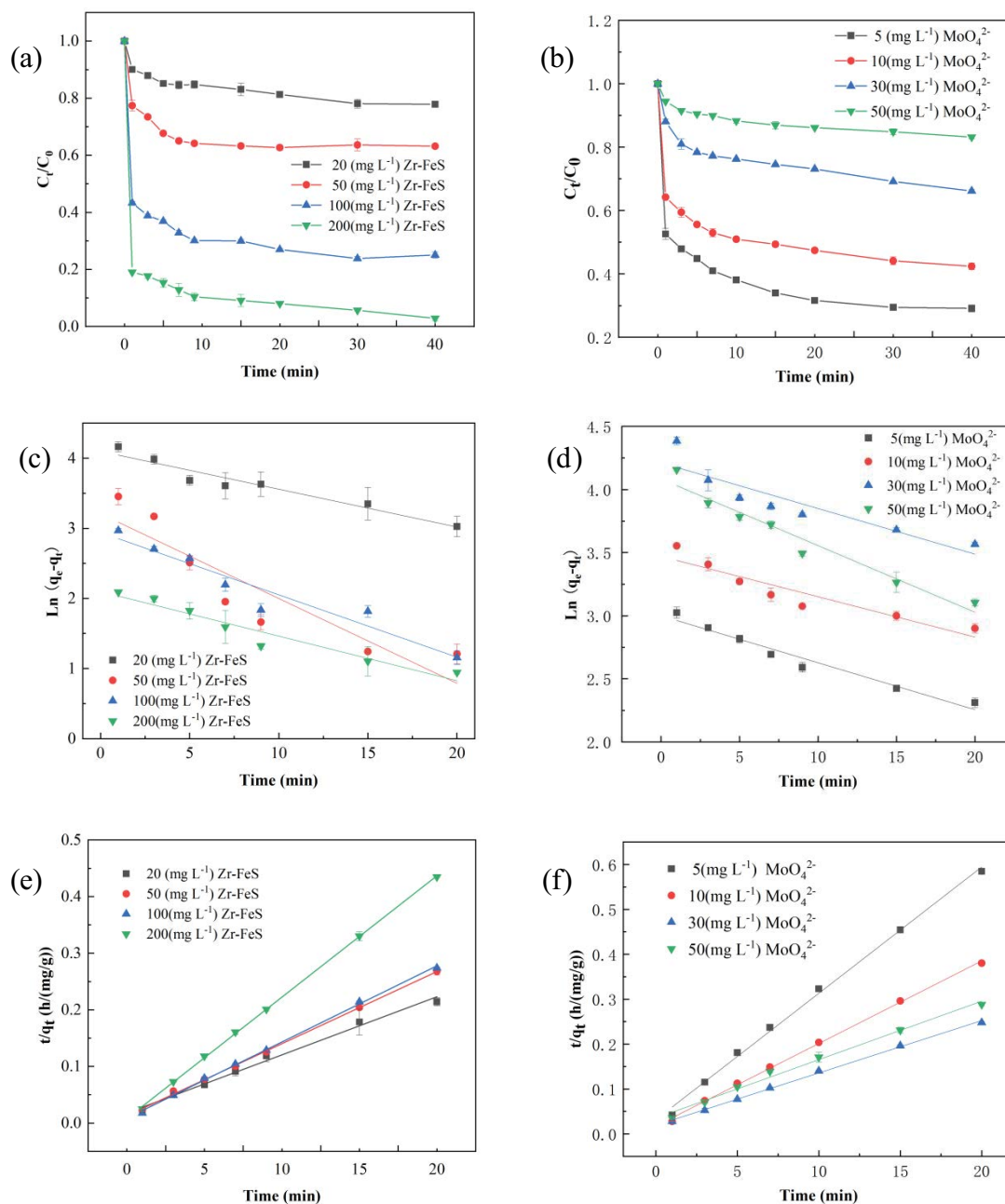


Fig. 3. Mo(VI) removal performance in systems with (a) different dose of Zr-FeS equal to 20, 50, 100 and 200 mg/L at an initial MoO_4^{2-} concentration of 10 mg/L, and (b) with Mo(VI) concentration of 5, 10, 30, and 50 mg/L at a dose of Zr-FeS equal to 100 mg/L; (c) and (d) are the pseudo-first-order kinetic fitting for systems (a) and (b), respectively (pH = 7.0, $T = 298$ K); (e) and (f) are the pseudo-second-order kinetic fitting for systems (a) and (b), respectively (pH = 7.0, $T = 298$ K).

changes in Zr-FeS before and after aging (Fig. 6b). The peaks at 17.0° and 30.0° indicated the presence of FeS (JCPDS, 15-0037) and ZrO_2 [40] on the Zr-FeS, respectively. The characteristic peaks of aged Zr-FeS at 2θ angles of 35.1° and 53.1° indicated the existence of lepidocrocite ($\gamma\text{-FeOOH}$), which may be related to the FeS/iron oxide layer electron transfer [39]. The above analysis illustrated that Zr-FeS showed a good anti-aging performance, which was convenient for the practical application of Mo(VI) removal.

3.7. Removal mechanism

3.7.1. Spectroscopy analysis

The Fourier-transform infrared spectroscopy (FTIR), XRD, and XPS analyses were conducted to further analyze Mo(VI) adsorption mechanism. As displayed in Fig. 6c, new diffraction peaks of $\text{Fe}_2(\text{MoO}_4)_3$ ($2\theta = 15.3^\circ$) (JCPDS No. 31-0642) and $\text{FeMo}_2\text{O}_6(\text{OH})_3$ ($2\theta = 23.1^\circ$, 26.8° , and 27.6°) (JCPDS No. 50-1619) were appeared in Zr-FeS after Mo(VI)

Table 1
Kinetic parameters of pseudo-first-order and pseudo-second-order for Mo(VI) adsorbed by Zr-FeS (pH = 7.0, T = 298 K)

Parameter		Initial dosage of Zr-FeS (mg/L)				Initial concentration of Mo(VI) (mg/L)			
		20	50	100	200	5	10	30	50
Pseudo-first-order	$q_{e,exp}$ (mg/g)	95.201	75.532	71.357	49.848	34.626	41.415	80.386	80.689
	$k_1 \times 10^{-2}$ (min ⁻¹)	0.054	0.121	0.089	0.064	0.037	0.032	0.036	0.053
	$q_{e,cal,1}$ (mg/g)	60.225	24.743	18.946	8.148	20.077	32.149	67.444	59.375
	R^2	0.924	0.796	0.912	0.924	0.954	0.855	0.792	0.943
Pseudo-second-order	$k_2 \times 10^{-2}$ (g/(mg·min))	0.006	0.013	0.212	0.057	0.025	0.020	0.007	0.005
	$q_{e,cal,2}$ (mg/g)	97.371	78.493	74.294	46.642	35.524	54.348	85.763	76.746
	R^2	0.989	0.998	0.998	0.999	0.996	0.998	0.998	0.989

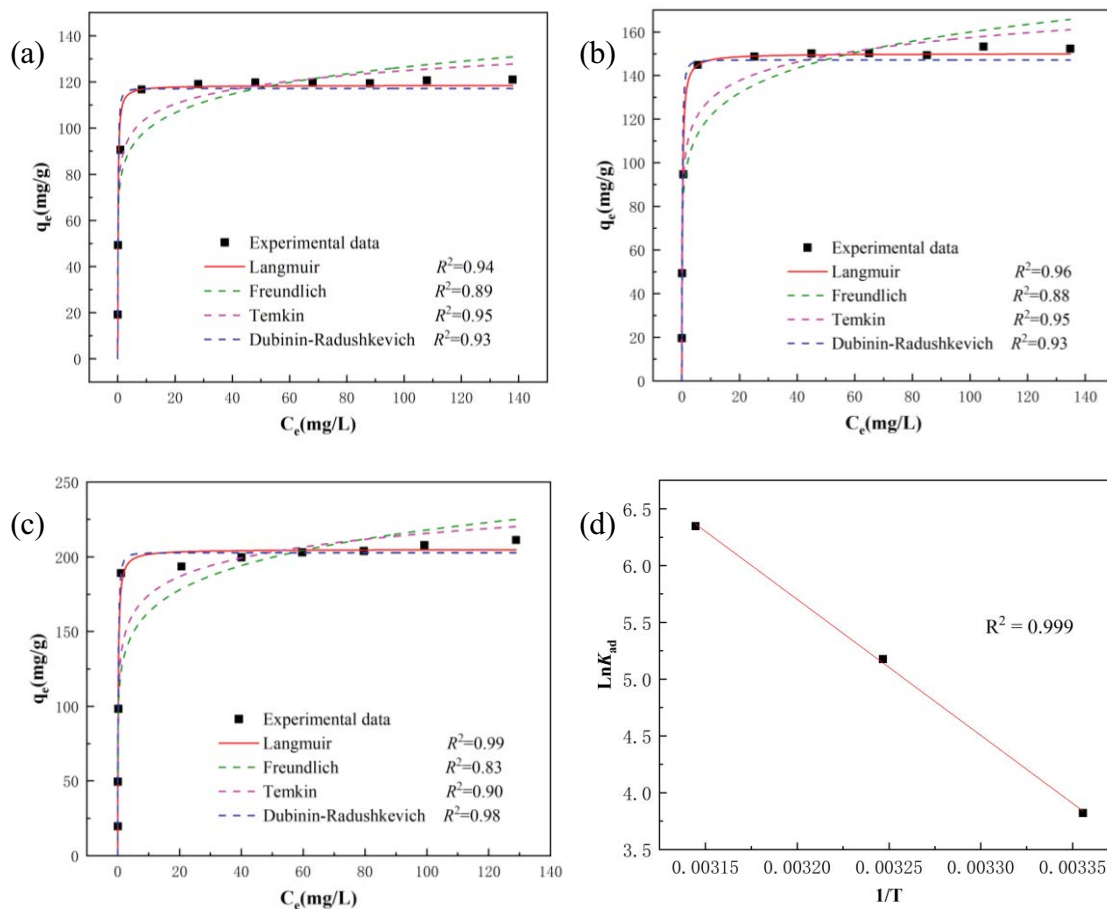


Fig. 4. Isotherms data and modeling of Mo(VI) adsorption on Zr-FeS at (a) 298 K, (b) 308 K, and (c) 318 K, (d) plot of $\ln K_{ad}$ vs. $1/T$; reaction conditions: Zr-FeS = 100 mg/L, pH = 7.0, shaking time = 24 h.

adsorption, which suggested that Mo was loaded on Zr-FeS surface by forming a complex with ferric ions [24]. The diffraction peak of ZrO_2 ($2\theta = 30.0^\circ$) can still be seen after Mo(VI) adsorption, which may be due to the role of ZrO_2 mainly as an electronic channel. As shown in Fig. 6d, the bands at 3,400 and 1,625 cm^{-1} belonged to the stretching vibration of O–H [41]. However, some adsorption peaks changed in the FTIR spectra of Mo-Zr-FeS after adsorbing Mo(VI). The 1,022 cm^{-1} adsorption peak might be allotted

to the bending vibrations of O–H [42]. The changes of these diffraction peaks between 1,000–1,300 cm^{-1} may be caused by the complex formed by O–H and molybdate, which suggested that O–H participated in the Mo(VI) removal.

Fig. 7a illustrates that the characteristic peak of Mo appeared at about 233 eV after reacting with Mo, which implied that Mo had been adsorbed on the Zr-FeS surface. FeS was the principal form of iron in Zr-FeS, because the Fe $2p_{3/2}$ peak at 710.5 eV is referred to FeS (Fig. 7b) [43].

Table 2

Isotherm adsorption model parameters for the removal of Mo(VI) by Zr-FeS, reaction conditions: initial Mo(VI) concentration = 10 mg/L, Zr-FeS = 100 mg/L and pH = 7.0

Isotherm models	Formula	Parameters	298 K	308 K	318 K
			$Q_{e,exp}$ (mg/g)	138.28	152.34
Langmuir	$\frac{C_e}{q_e} = \frac{C_e}{Q_m} + \frac{1}{Q_m b}$	Q_m (mg/g)	118.48	150.13	205.01
		k_L (L/mg)	7.88	4.91	6.16
		$R_L \times 10^2$	0.08–5.96	0.14–9.25	0.11–7.51
		R^2	0.95	0.96	0.99
Freundlich	$\ln q_e = \frac{1}{n} \ln C_e + \ln K_F$	k_F (mg ¹⁻ⁿ ·L ⁿ /g)	77.57	93.35	121.83
		n	9.43	8.38	7.91
		R^2	0.89	0.88	0.83
Temkin	$q_e = \frac{RT}{bT} \ln A + \frac{RT}{bT} \ln C_e$	$A \times 10^4$ (L/mg)	1.12	3.93	1.64
		b_T (kJ/mol)	0.11	0.082	0.056
		R^2	0.95	0.95	0.98
Dubinin–Radushkevich	$\ln Q_e = \ln Q_m - \beta_L \varepsilon^2$	Q_0 (mg/g)	117.12	147.11	202.82
		β_L (mol ² /(kJ ²))	0.13	0.17	0.17
		E (kJ/mol)	1.97	1.74	1.71
		R^2	0.90	0.90	0.92

Table 3

Comparison of Zr-FeS and other adsorbents for Mo(VI) adsorption capacity

Adsorbents	Adsorption capacity (mg/g)	References
Nanomagnetic CuFe ₂ O ₄	30.58	[12]
Modified pomelo peel	48.54	[35]
Maghemite nanoparticles	33.4	[36]
NaOCl-oxidized multi-walled carbon nanotubes	22.73	[13]
Modified drinking water treatment residues	43.67	[34]
Modified mesoporous zirconium silicates	22.8	[37]
Zirconium modified FeS	118.48–205.01	Present study

Table 4

Thermodynamic parameters for Mo(VI) adsorption onto Zr-FeS

Temperature (K)	ΔG° (kJ/mol)	ΔH° (kJ/mol)	ΔS° (J/(mol·K))	R^2
298	-9.469			
308	-13.254	99.552	365.993	0.999
318	-16.784			

However, the peak value of Fe 2p_{3/2} shifted from 710.5 to 711.0 eV after the Mo(VI) adsorption, indicating that some divalent iron lost electrons and changed into trivalent iron (Fe(III)-S) [44]. The two peaks with 161.3 and 162.5 eV in the S 2p_{3/2} were referred to S²⁻ and S₂²⁻, respectively (Fig. 7c) [45]. Besides, the peaks at 163.3 and 164.6 eV represented polysulfide (S_n²⁻), and the peaks at 166.9 and 168.3 eV referred to SO₃²⁻ and SO₄²⁻ [46]. In Zr(3d) spectrum, there were two peaks with 182.8 and 185.3 eV (Fig. 7d), indicating that Zr existed in the form of a positive tetravalent [47]; the valence state of Zr did not change significantly after Mo(VI) adsorption. The three peaks with 529.7, 531.1, and

532.8 eV in the O(1s) spectrum referred to metal-O, O-S/O=C, and O-H, respectively (Fig. 7e) [47]. After adsorbing Mo(VI), the disappearance of the O-H peak indicated that it participated in the adsorption. The Mo(3d) peaks at 235.7 and 232.5 eV were ascribed to the presence of Mo(VI) (Fig. 7f) [48]. Therefore, there existed no redox reaction during the whole Mo(VI) removal process.

3.7.2. Calculations of DFT

Previous publications have found that the surface of FeS(001) was found to be more stable [49], so the FeS(001) surface was cut and the FeS model was constructed. Then a 3 × 3 × 1 supercell was built and the vacuum slab was adjusted to 20 Å to avoid interaction (Fig. 8a). To investigate the the removal mechanism of Mo by Zr-doped FeS(001), the Fe atom in FeS(001) was replaced by Zr to obtain a Zr-doped FeS(001) structure, and this structure was represented by Zr/FeS (001) (Fig. 8b). According to the structure optimization results, the binding energy of Zr to defective FeS(001) is -2.95 eV (Table S2) when FeS(001) was doped with Zr atoms.

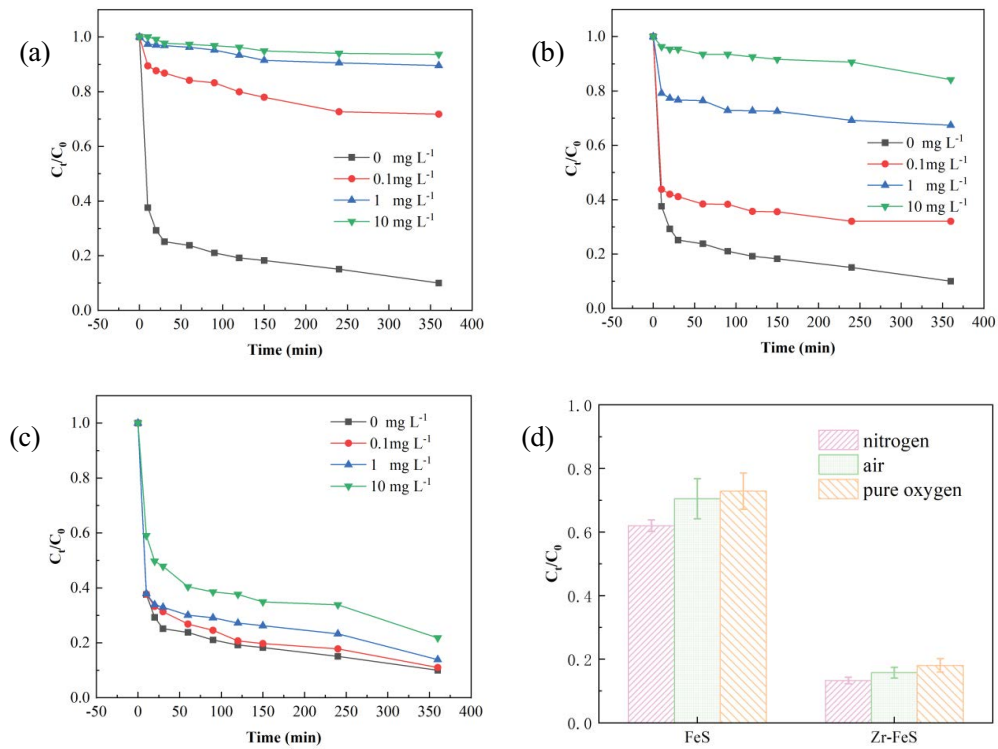


Fig. 5. Effect of (a) PO_4^{3-} , (b) HCO_3^- , and (c) SO_4^{2-} on Mo(VI) removal at different concentrations and (d) dissolved oxygen conditions on Mo(VI) removal by FeS and Zr-FeS.

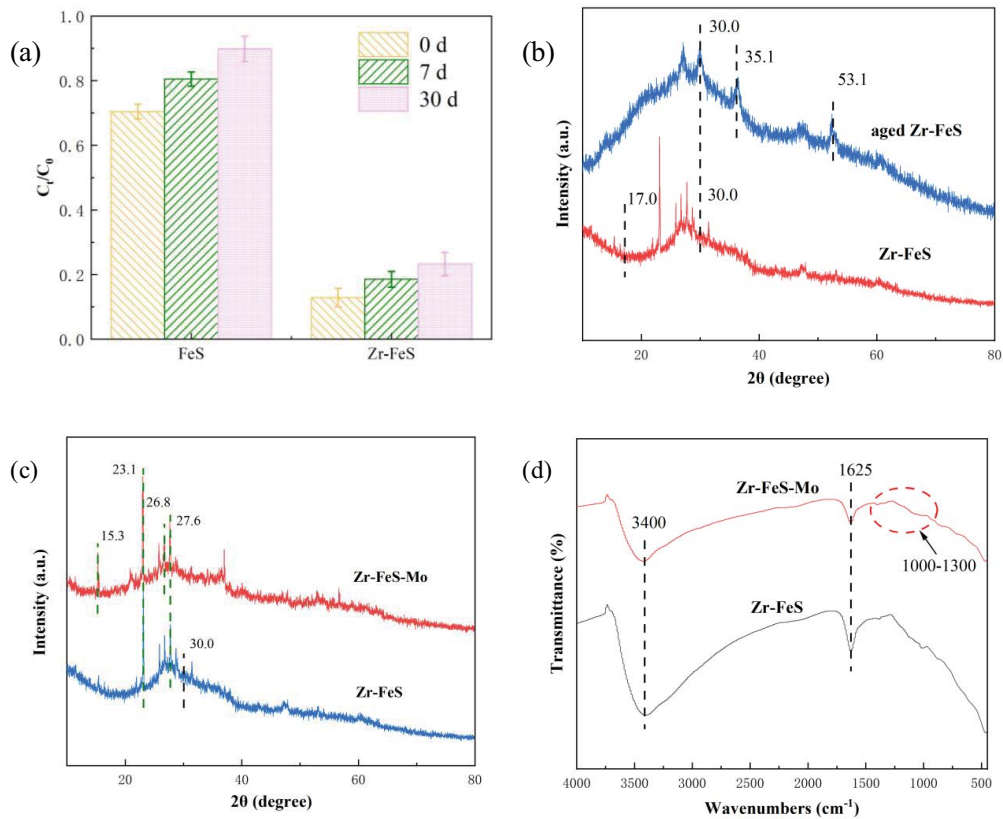


Fig. 6. (a) Effect of aging on the removal efficiency of Mo(VI) by FeS and Zr-FeS; (b) X-ray diffraction analysis of Zr-FeS, and aged Zr-FeS (30 d); (c) X-ray diffraction and (d) Fourier-transform infrared spectra of the bare Zr-FeS and Mo(VI)-loaded Zr-FeS.

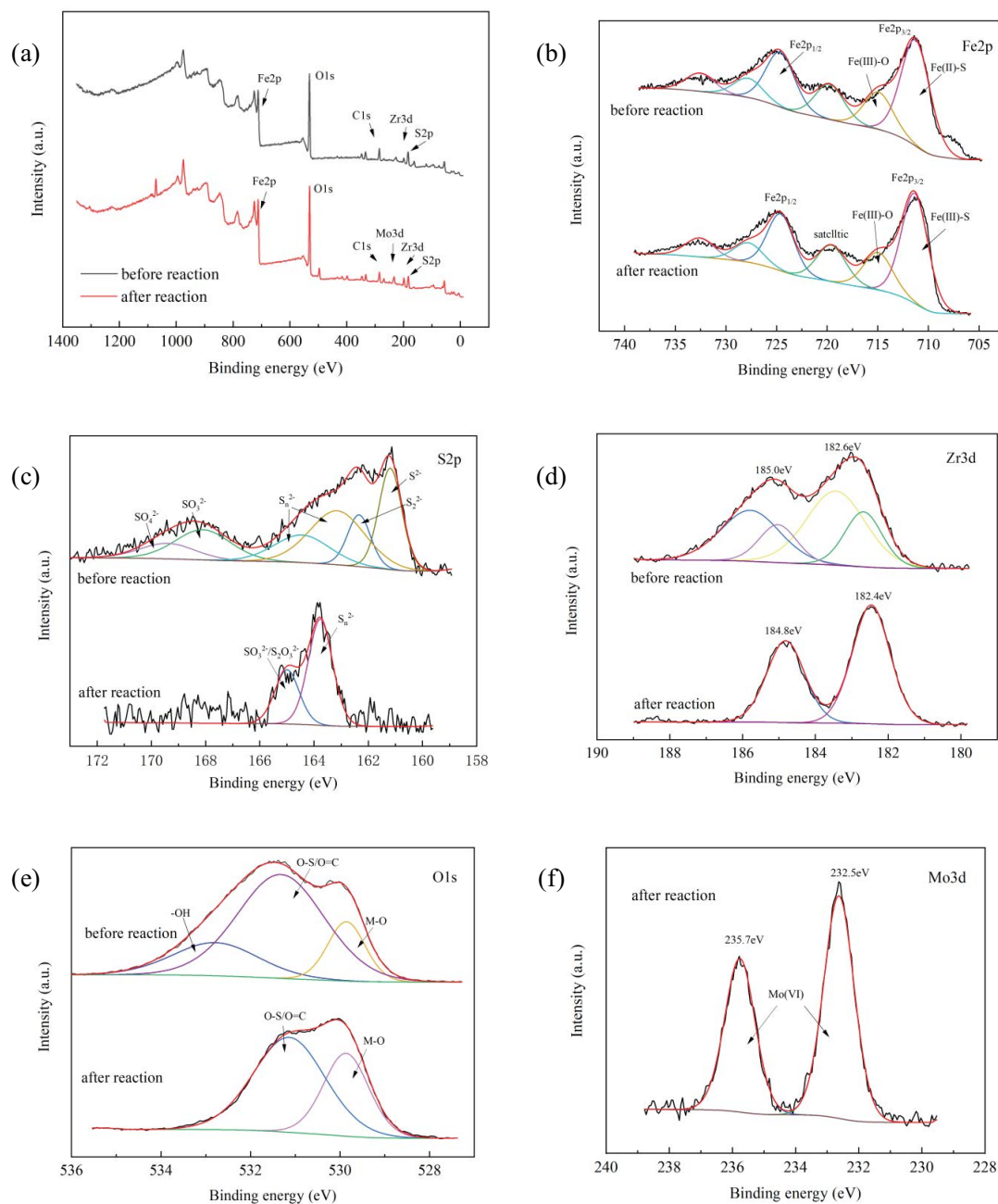


Fig. 7. (a) X-ray photoelectron spectroscopy full spectrum, (b) Fe2p, (c) S2p, (d) Zr3d, (e) O1s (M: metals), and (f) Mo3d spectra of the Zr-FeS before and after reaction with Mo(VI) (Mo(VI) concentration = 10 mg/L, Zr-FeS = 100 mg/L, Zr/Fe = 0.5, pH = 7.0).

Then, the adsorption of Mo on the pristine FeS(001) and Zr/FeS (001) surfaces were further studied. Mo's most stable adsorption sites are hole sites of the four S, which have the lowest E_{ads} (-7.09 eV) (Fig. 8c). Mo bonded to Fe and S, and the bond lengths of Mo-Fe (2.595 Å) and Mo-S (2.530 Å), respectively. Following the adsorption on the surface of Zr/FeS (001), when Mo was the most stable adsorption sites are the hole sites of the four S and the E_{ads} are the lowest (-7.61 eV) (Table S3). The Mo atom was bonded with Fe, S, and Zr at the same time, with bond lengths of Mo-Fe (2.540 Å), Mo-S (2.415 Å), and Mo-Zr (2.710 Å),

respectively, the most stable adsorption structure as shown in the Fig. 8d. By comparison, after Zr was doped, the bond length of Mo-Fe and Mo-S increased significantly, Mo-Fe bond length rose by 0.055 Å, Mo-S bond length grew by 0.115 Å. The Zr-doped makes it helps Mo to connect to the Zr/FeS(001) surface. Mo atoms create Mo-Zr bond (2.710 Å) with the Zr atom making Mo more securely adsorbed on the Zr/FeS(001) surface. According to some evidence, Zr/FeS(001) provides a more stable adsorption site for Mo than FeS(001), and this is owing to the difference in favor of bond lengths.

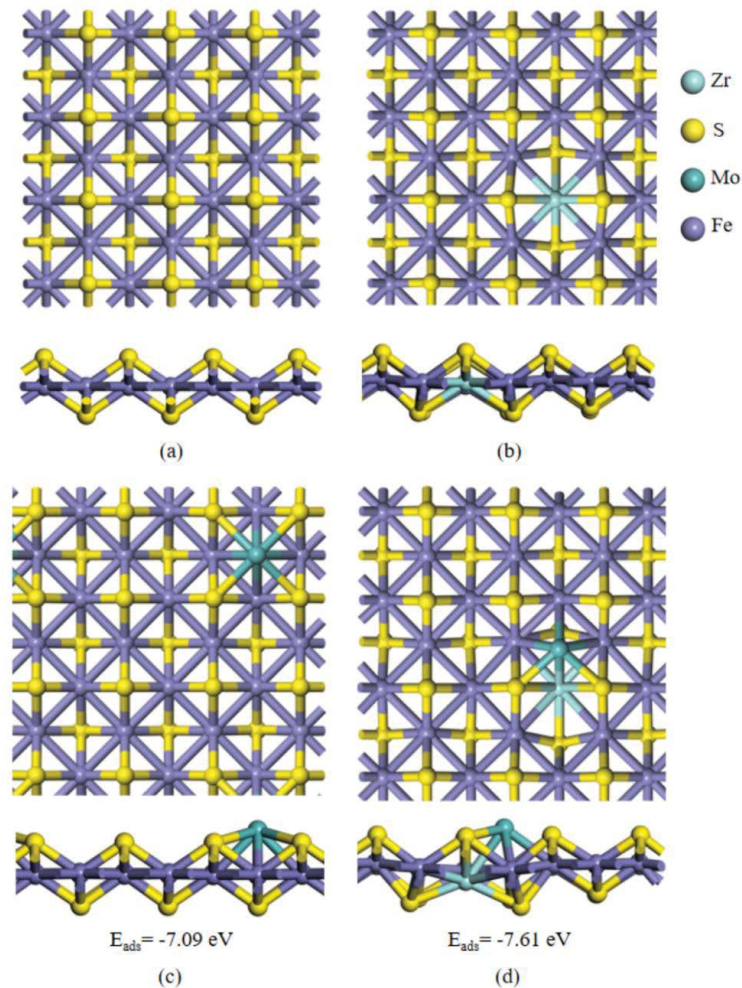


Fig. 8. Schematic illustration of (a) the top view of the geometry-optimized structures of FeS(001) surface, (b) the most stable structure of Zr-doped FeS(001), (c) the best adsorption site of Mo on the pristine FeS(001) surface, and (d) Zr-FeS(001) surface.

To further clarify the interaction mechanism between adsorbate and substrate, the differential charge densities of Mo@FeS(001) and Mo@Zr-FeS(001) were also determined (Fig. 9). Yellow and blue regions suggest accumulation and depletion of charge. As for Mo@FeS(001), although having a sizable area of electron enrichment near the Mo atom, there were also more electron deficient areas outside the Fe surface (Fig. 9a and b), which subsequently results in weak interaction with the Mo atom. As observed in Fig. 9c and d, doped Zr may greatly boost charge transfer on the surface of Mo@Zr-FeS(001), it further caused an imbalanced charge distribution at the interphase and strong charge interaction between Mo and Zr-FeS(001). Electron charge density difference also confirmed that a larger electron enrichment area is found between Mo and Zr atoms in Mo@Zr-FeS(001), favoring the development of a stronger Mo-Zr bond in Mo@Zr-FeS(001) when compared to Mo-FeS(001). According to our DFT calculation results, the mechanism of the reconstructed Mo@Zr-FeS(001) suggested that the doped Zr atom on FeS(001) enhanced charge transfer to the development of a stronger Mo-Zr bond and promoted the strong Mo adsorption on the Zr-FeS(001) surface.

The Zr-FeS inhibits the aggregation of FeS particles through electrostatic repulsion or spatial effects, thereby increasing the specific surface area and reactivity of ferrous sulfide. The adsorption kinetics of Mo(VI) were consistent with the pseudo-second-order adsorption kinetic model, indicating that chemisorption was participated in the adsorption process. According to the XPS analysis, the mechanism for removing Mo(VI) by the Zr-FeS was adsorption because only the characteristic peak of Mo(VI) was found. Combined with the analysis results of the FTIR, XRD, XPS, and DFT calculation, the main mechanisms for Mo(VI) removal were hydrogen bonding, electrostatic interaction, as well as surface complexation. The adsorption mechanism of Mo(VI) on Zr-FeS is shown in Fig. 10.

3.8. Regeneration

The reusability is a crucial factor for judging the stability of an adsorbent. A good adsorbent should have properties of high adsorption capacity and high desorption efficiency, thereby reducing their economic costs. Therefore, 0.1 M NaOH solution was used for elution, which was more

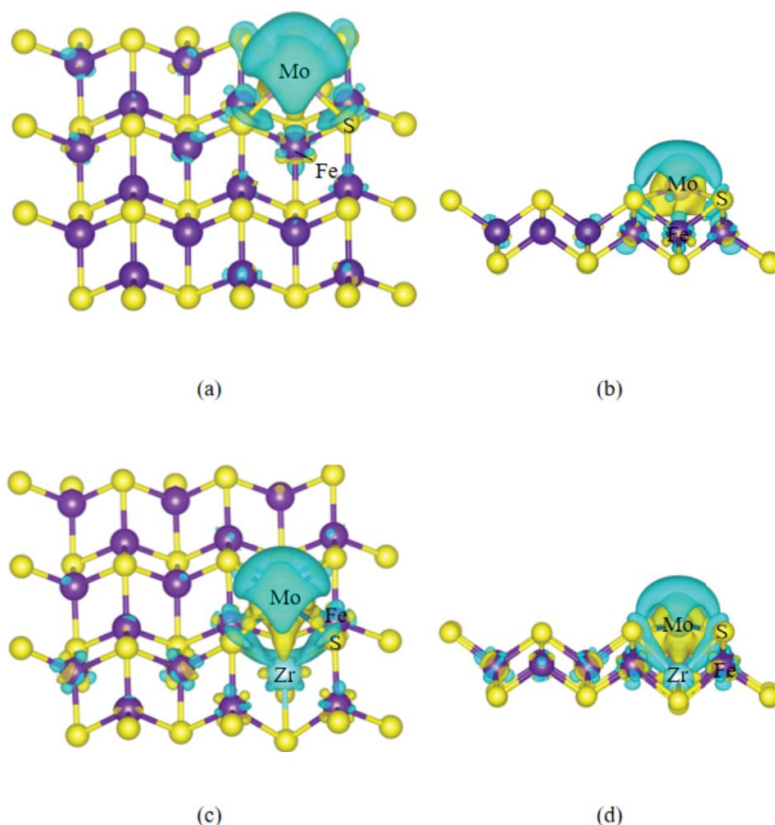


Fig. 9. (a) and (b) Differential charge density map of Mo-FeS(001) system; (c) and (d) differential charge density map of Mo@Zr-FeS(001) system.



Fig. 10. Proposed mechanism for the adsorption of Mo(VI) onto Zr-FeS.

favorable to Mo(VI) desorption according to the similar consistency principle and electrostatic repulsion [50]. Five consecutive cycles of adsorption/desorption were carried out for Mo(VI) on Zr-FeS. As shown in Fig. 11, the removal rate of Zr-FeS was still higher than 86.02% after five times

of regeneration, and the desorption rate also stabilized around 79.55%. The reason for the slight decrease in the adsorption amount might be the incomplete desorption of Mo(VI) on Zr-FeS, which was caused by both physisorption and chemisorption [51].

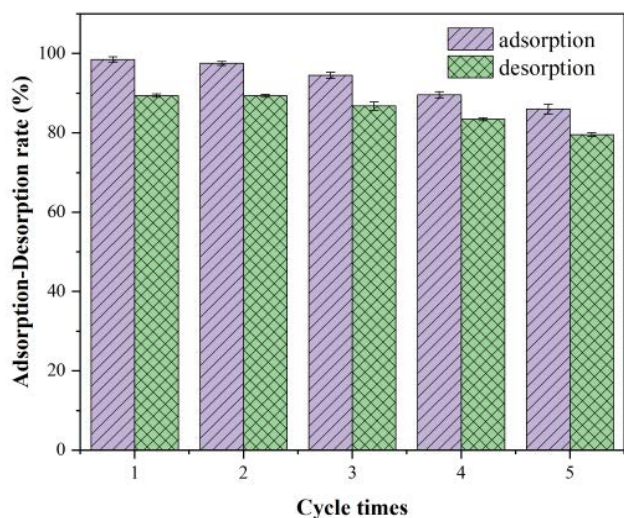


Fig. 11. Performance of Zr-FeS by multiple cycles of regeneration. Conditions: Zr-FeS dosage = 5.0 g/L, $T = 298$ K, initial Mo concentration = 30 mg/L.

3.9. Implications

Iron sulfide has been universally used for removing organic pollutants and heavy metals in sewage due to its strong reduction performance. But FeS is easy to be deactivated due to agglomeration and oxidation in the process of synthesis, storage, and use, which will affect its practical application performance. In this study, zirconia was used to modify FeS nanoparticles to solve the above problems. The results indicated that Mo(VI) adsorption process could reach balance within 40 min, and the optimal adsorption capacity could be reached to 118.48 mg/g at 298 K, which was significantly higher than the current results. The competitive anions had certain inhibition on the Mo(VI) adsorption. The Zr-FeS had better resistance to oxidation and aging. Spectroscopy analysis and DFT calculations further confirmed that physisorption and chemisorption were the dominant forces for Mo(VI) removal. Compared to nano-FeS, Zr-FeS has greater application potential in treating Mo-containing (VI) wastewater.

4. Conclusions

Mo(VI) could be quickly and efficiently removed by Zr-FeS with Zr/Fe = 0.5 from the aquatic solutions. The Mo(VI) adsorption process conformed to the pseudo-second-order kinetic model and the Langmuir model. The removal rate of Mo(VI) was higher than 90% at pH of 4.0, and the largest adsorption capacity reached 118.48 mg/g at 298 K. The adsorption process was a spontaneous, feasible, and endothermic process. Competing anions (such as PO_4^{3-} , HCO_3^- , and SO_4^{2-}) had certain inhibition on the Mo(VI) adsorption. Zr-FeS had excellent anti-aging and oxidation properties. The spectroscopy analysis and DFT calculation results showed that physical adsorption and chemisorption were the main mechanisms for the removal of Mo(VI). All in all, Zr-FeS could be a suitable and beneficial material for adsorbing Mo(VI) removal from the aquatic solutions.

Acknowledgment

This work was supported by the National Natural Science Foundation of China (No. 51709001), the Nature Science Foundation of Anhui Province of China (No. 2208085ME154), Shandong Provincial Natural Science Foundation (No. ZR2021QE272), and the Open Project of Engineering Research Center of Biofilm Water Purification and Utilization Technology of Ministry of Education (BWPU2021KF08).

References

- [1] C. Ma, A. Vasileiadis, H.T. Wolterbeek, A.G. Denkova, P. Serra Crespo, Adsorption of molybdenum on Zr-based MOFs for potential application in the $^{99}\text{Mo}/^{99\text{m}}\text{Tc}$ generator, *Appl. Surf. Sci.*, 572 (2022) 151340, doi: 10.1016/j.apsusc.2021.151340.
- [2] W.R. Chappell, R.R. Meglen, R. Moure-Eraso, C.C. Solomons, T.A. Tsongas, P.A. Walravens, P.W. Winston, Human Health Effects of Molybdenum in Drinking Water, U.S. EPA Report, 1979.
- [3] A.Y. Ahmad, M.A. Al-Ghouti, M. Khraisheh, N. Zouari, Insights into the removal of lithium and molybdenum from groundwater by adsorption onto activated carbon, bentonite, roasted date pits, and modified-roasted date pits, *Bioresour. Technol.*, 18 (2022) 101045, doi: 10.1016/j.biteb.2022.101045.
- [4] L.W. Yao, Y.H. Liu, K. Yang, X. Xi, R.Q. Niu, C. Ren, C.S. Wang, Spatial-temporal analysis and background value determination of molybdenum concentration in basins with high molybdenum geochemical background – a case study of the Upper Yi River Basin, *J. Environ. Manage.*, 286 (2021) 112199, doi: 10.1016/j.jenvman.2021.112199.
- [5] I. Timofeev, N. Kosheleva, N. Kasimov, Contamination of soils by potentially toxic elements in the impact zone of tungsten-molybdenum ore mine in the Baikal region: a survey and risk assessment, *Sci. Total Environ.*, 642 (2018) 63–76.
- [6] G. Tepanosyan, L. Sahakyan, C. Zhang, A. Saghatelian, The application of local Moran's I to identify spatial clusters and hot spots of Pb, Mo and Ti in urban soils of Yerevan, *Appl. Geochem.*, 104 (2019) 116–123.
- [7] Z. Wang, C. Hong, Y. Xing, K. Wang, Y. Li, L. Feng, S. Ma, Spatial distribution and sources of heavy metals in natural pasture soil around copper-molybdenum mine in Northeast China, *Ecotoxicol. Environ. Saf.*, 154 (2018) 3296, doi: 10.1016/j.ecoenv.2018.02.048.
- [8] J. Baltrusaitis, B. Mendoza-Sanchez, V. Fernandez, R. Veenstra, N. Dukstiene, A. Roberts, N. Fairley, Generalized molybdenum oxide surface chemical state XPS determination via informed amorphous sample model, *Appl. Surf. Sci.*, 326 (2015) 151–161.
- [9] R. Gamal, S.E. Rizk, N.E. El-Hefny, The adsorptive removal of Mo(VI) from aqueous solution by a synthetic magnetic chromium ferrite nanocomposite using a nonionic surfactant, *J. Alloys Compd.*, 853 (2021) 157039, doi: 10.1016/j.jallcom.2020.157039.
- [10] F. Guo, X.L. Xi, L.W. Ma, Z.R. Nie, Property and mechanism on sorption of molybdenum from tungstate solution with a porous amine resin, *J. Cleaner Prod.*, 335 (2022) 130304, doi: 10.1016/j.jclepro.2021.130304.
- [11] S.H.R. Rouhani, R. Davarkhah, P. Zaheri, S.M.A. Mousavian, Separation of molybdenum from spent HDS catalysts using emulsion liquid membrane system, *Chem. Eng. Process.*, 153 (2020) 107958, doi: 10.1016/j.cep.2020.107958.
- [12] Y.J. Tu, T.S. Chan, H.W. Tu, S.L. Wang, C.F. You, C.K. Chang, Rapid and efficient removal/recovery of molybdenum onto ZnFe_2O_4 nanoparticles, *Chemosphere*, 148 (2016) 452–458.
- [13] Y.C. Chen, C.Y. Lu, Kinetics, thermodynamics and regeneration of molybdenum adsorption in aqueous solutions with NaOCl-oxidized multiwalled carbon nanotubes, *J. Ind. Eng. Chem.*, 20 (2014) 2521–2527.
- [14] B. Verbinen, C. Block, P. Lievens, A. Van Brecht, C. Vandecasteele, Simultaneous removal of molybdenum,

- antimony and selenium oxyanions from wastewater by adsorption on supported magnetite, *Waste Biomass Valorization*, 4 (2013) 635–645.
- [15] B.C. Bostick, S. Fendorf, Differential adsorption of molybdate and tetrathiomolybdate on pyrite (FeS₂), *Environ. Sci. Technol.*, 37 (2003) 285–291.
- [16] J.J. Lian, H.L. Wang, H.P. He, W.L. Huang, M. Yang, Y. Zhong, P.A. Peng, The reaction of amorphous iron sulfide with Mo(VI) under different pH conditions, *Chemosphere*, 266 (2021) 128946, doi: 10.1016/j.chemosphere.2020.128946.
- [17] M. Xiao, X. Lai, J. He, J. Huang, Z. Tang, R. Wu, J. Jian, Highly efficient removal of aqueous Hg(II) by FeS micro-flakes, *Sci. Total Environ.*, 870 (2023) 162013, doi: 10.1016/j.scitotenv.2023.162013.
- [18] Y. Sun, Y. Liu, Z. Lou, K. Yang, D. Lv, J. Zhou, S.A. Baig, X. Xu, Enhanced performance for Hg(II) removal using biomaterial (CMC/gelatin/starch) stabilized FeS nanoparticles: stabilization effects and removal mechanism, *Chem. Eng. J.*, 344 (2018) 616–624.
- [19] H. Wu, J.J. Chen, L.X. Xu, X.J. Guo, P. Fang, K. Du, C. Shen, G.D. Sheng, Decorating nanoscale FeS onto metal–organic framework for the decontamination performance and mechanism of Cr(VI) and Se(IV), *Colloids Surf., A*, 625 (2021) 126887, doi: 10.1016/j.colsurfa.2021.126887.
- [20] Z. Wang, M.C. Xing, W.K. Fang, D.Y. Wu, One-step synthesis of magnetite core/zirconia shell nanocomposite for high efficiency removal of phosphate from water, *Appl. Surf. Sci.*, 366 (2016) 67–77.
- [21] A. Teimouri, S.G. Nasab, N. Vandatpoor, S. Habibollahi, H. Salavati, A.N. Chermahini, Chitosan/zeolite Y/nano ZrO₂ nanocomposite as an adsorbent for the removal of nitrate from the aqueous solution, *Int. J. Biol. Macromol.*, 93 (2016) 254–266.
- [22] D.D. Zhao, Y. Yu, J.P. Chen, Fabrication and testing of zirconium-based nanoparticle doped activated carbon fiber for enhanced arsenic removal in water, *RSC Adv.*, 6 (2016) 27020–27030.
- [23] Y.-W. Wu, J. Zhang, J.-F. Liu, L. Chen, Z.-L. Deng, M.-X. Han, X.-S. Wei, A.-M. Yu, H.-L. Zhang, Fe₃O₄@ZrO₂ nanoparticles magnetic solid phase extraction coupled with flame atomic absorption spectrometry for chromium(III) speciation in environmental and biological samples, *Appl. Surf. Sci.*, 258 (2012) 6772–6776.
- [24] H.Y. Wu, Y.T. Liu, B. Chen, F. Yang, L.M. Wang, Q.P. Kong, T.R. Ye, J.J. Lian, Enhanced adsorption of molybdenum(VI) from aquatic solutions by chitosan-coated zirconium–iron sulfide composite, *Sep. Purif. Technol.*, 279 (2021) 119736, doi: 10.1016/j.seppur.2021.119736.
- [25] G. Kresse, J. Furthmüller, Efficient iterative schemes for *ab initio* total-energy calculations using a plane-wave basis set, *Phys. Rev. B: Condens. Matter*, 54 (1996) 11169–11186.
- [26] G. Kresse, J. Hafner, *Ab initio* molecular dynamics for liquid metals, *Phys. Rev. B: Condens. Matter*, 47 (1993) 222–229.
- [27] J.P. Perdew, K. Burke, M. Ernzerhof, Generalized gradient approximation made simple, *Phys. Rev. Lett.*, 77 (1996) 3865–3868.
- [28] G. Kresse, D. Joubert, From ultrasoft pseudopotentials to the projector augmented-wave method, *Phys. Rev. B: Condens. Matter*, 59 (1999) 1758–1775.
- [29] P.E. Blöchl, Projector augmented-wave method, *Phys. Rev. B: Condens. Matter*, 50 (1994) 17953–17979.
- [30] H.J. Monkhorst, J.D. Pack, Special points for Brillouin-zone integrations, *Phys. Rev. B: Condens. Matter*, 13 (1976) 1746–1747.
- [31] G. Kim, G. Kwon, H. Lee, The role of surface hydroxyl groups on a single-atomic Rh₁/ZrO₂ catalyst for direct methane oxidation, *Chem. Commun.*, 57 (2021) 1671–1674.
- [32] Y. Sun, Z. Lou, J. Yu, X. Zhou, D. Lv, J. Zhou, S.A. Baig, X. Xu, Immobilization of mercury(II) from aqueous solution using Al₂O₃-supported nanoscale FeS, *Chem. Eng. J.*, 323 (2017) 483–491.
- [33] A.J. Varma, S.V. Deshpande, J.F. Kennedy, Metal complexation by chitosan and its derivatives: a review, *Carbohydr. Polym.*, 55 (2004) 77–93.
- [34] J.J. Lian, F.J. Zhou, B. Chen, M. Yang, S.S. Wang, Z.L. Liu, S.P. Niu, Enhanced adsorption of molybdenum(VI) onto drinking water treatment residues modified by thermal treatment and acid activation, *J. Cleaner Prod.*, 244 (2020) 118719, doi: 10.1016/j.jclepro.2019.118719.
- [35] J.J. Lian, Y.G. Huang, B. Chen, S.S. Wang, P. Wang, S.P. Niu, Z.L. Liu, Removal of molybdenum(VI) from aqueous solutions using nano zero-valent iron supported on biochar enhanced by cetyl-trimethyl ammonium bromide: adsorption kinetic, isotherm and mechanism studies, *Water Sci. Technol.*, 2017 (2018) 859–868.
- [36] A. Afkhami, A.R. Norooz, Removal, preconcentration and determination of Mo(VI) from water and wastewater samples using maghemite nanoparticles, *Colloids Surf., A*, 346 (2009) 52–57.
- [37] H. Sepeshrian, S. Waqif-Husain, J. Fasihi, M.K. Mahani, Adsorption behavior of molybdenum on modified mesoporous zirconium silicates, *Sep. Sci. Technol.*, 45 (2010) 421–426.
- [38] D. Lv, J.S. Zhou, Z. Cao, J. Xu, Y.L. Liu, Y.Z. Li, K.L. Yang, Z.M. Lou, L.P. Lou, X.H. Xu, Mechanism and influence factors of chromium(VI) removal by sulfide-modified nanoscale zerovalent iron, *Chemosphere*, 224 (2019) 306–315.
- [39] L.J. Wang, M.X. Wang, Z.J. Li, Y.Y. Gong, Enhanced removal of trace mercury from surface water using a novel Mg₂Al layered double hydroxide supported iron sulfide composite, *Chem. Eng. J.*, 393 (2020) 124635, doi: 10.1016/j.cej.2020.124635.
- [40] T. Zeeshan, M.T. Qureshi, Z.N. Kayani, A. Arshad, F. Ullah, R.A. Hameed, H. Ragab, N. Alam, W. Rehman, M. Saleem, A comparative computational and experimental study of Al-ZrO₂ thin films for optoelectronic applications, *Solid State Commun.*, 358 (2022) 115006, doi: 10.1016/j.ssc.2022.115006.
- [41] H.R. Dong, C. Zhang, J.M. Deng, Z. Jiang, L.H. Zhang, Y.J. Cheng, K.J. Hou, L. Tang, G.M. Zeng, Factors influencing degradation of trichloroethylene by sulfide-modified nanoscale zero-valent iron in aqueous solution, *Water Res.*, 135 (2018) 1–10.
- [42] Z. Chen, H. Luo, H. Rong, Development of polyaminated chitosan-zirconium(IV) complex bead adsorbent for highly efficient removal and recovery of phosphorus in aqueous solutions, *Int. J. Biol. Macromol.*, 164 (2020) 1183–1193.
- [43] D.X. Qian, Y.M. Su, Y.X. Huang, H.Q. Chu, X.F. Zhou, Y.L. Zhang, Simultaneous molybdate (Mo(VI)) recovery and hazardous ions immobilization via nanoscale zerovalent iron, *J. Hazard. Mater.*, 344 (2018) 698–706.
- [44] Y.Z. Song, W. Zhang, J. Chen, Y.T. Lu, J. Song, L.L. Zhang, J.M. Xie, Y. Ye, Synthesis of FeS nanoparticles for the catalytic reduction of 2,4-dinitrochlorobenzene, *Russ. J. Phys. Chem. A*, 94 (2020) 1184–1189.
- [45] J. Duan, H.D. Ji, X. Zhao, S.T. Tian, X.N. Liu, W. Liu, D.Y. Zhao, Immobilization of U(VI) by stabilized iron sulfide nanoparticles: water chemistry effects, mechanisms, and long-term stability, *Chem. Eng. J.*, 393 (2020) 124692, doi: 10.1016/j.cej.2020.124692.
- [46] J. Su, H. Hao, X. Lv, X. Jin, Q. Yang, Properties and mechanism of hexavalent chromium removal by FeS@graphite carbon nitride nanocomposites, *Colloids Surf., A*, 597 (2020) 124751, doi: 10.1016/j.colsurfa.2020.124751.
- [47] X.Z. Wang, S.L. Pan, M. Zhang, J.W. Qi, X.Y. Sun, C. Gu, L.J. Wang, J.S. Li, Modified hydrous zirconium oxide/PAN nanofibers for efficient defluorination from groundwater, *Sci. Total Environ.*, 685 (2019) 401–409.
- [48] J.J. Lian, M. Yang, S.S. Wang, B. Chen, F.J. Zhou, Z.L. Liu, Treatment of molybdenum(VI)-containing groundwater using chitosan nanoparticle: adsorption mechanism and performances, *Desal. Water Treat.*, 167 (2019) 258–268.
- [49] D.Y. Dzade, N.H. de Leeuw, Activating the FeS(001) surface for CO₂ adsorption and reduction through the formation of sulfur vacancies: a DFT-D3 study, *Catalysts*, 11 (2021) 127, doi: 10.3390/catal11010127.
- [50] J. Li, Q. Zhang, J. Feng, W. Yan, Synthesis of PPy-modified TiO₂ composite in H₂SO₄ solution and its novel adsorption characteristics for organic dyes, *Chem. Eng. J.*, 225 (2013) 766–775.
- [51] C.Y. Chen, J.C. Chang, A.H. Chen, Competitive biosorption of azo dyes from aqueous solution on the templated crosslinked chitosan nanoparticles, *J. Hazard. Mater.*, 185 (2011) 430–441.

Supplementary information

S1. Analytical methods

The surface characteristics of the FeS and Zr-FeS before and after the adsorption of Mo(VI) were measured using Nova NanoSEM 430 (FEI, USA). Fourier-transform infrared (FTIR) spectra were recorded on a Nicolet 6700 FTIR spectrophotometer. Powder X-ray diffraction patterns at 2θ angles from 10° to 80° were recorded at an interval of 0.33° on an Ultima IV diffractometer using Cu radiation (40 kV, 40 mA). Through the N_2 adsorption/desorption test, the V-Sorb 2800P surface area and pore distribution analyzer

was used to analyze the specific surface area of Brunauer–Emmett–Teller. The chemical states of the surface elements of the Zr-FeS before and after reaction with Mo(VI) were recorded by X-ray photoelectron spectroscopy using monochromatic Al K X-ray radiation (ESCALAB 250Xi, Thermo, USA). The pH at the point of zero charges (pH_{pzc}) of the materials was determined using the solid addition method as described elsewhere (Fotsing et al. [S1]). The concentrations of Mo and total Fe were determined by flame atomic absorption spectrometer (PinAAcle 900T, PerkinElmer, USA).

Table S1
Soil pollution condition of Mo(VI) in different parts of the world

Region	Soil properties	Mo content (mg/kg)		Literature source
		Mean	Maximum	
Luanchuan County, Henan	Mining soil	28.19	343	[4]
Lake Baikal	Residential areas	223	420	[5]
	Relaxation area	293	430	
Yerevan	Urban soil	2.6	421	[6]
Hulun Buir	Natural pasture soil	1.53	3.77	[7]

Table S2
Optimization results of Zr atom doping at FeS sites (001). The atoms of zirconium, iron, and sulfur are represented by the light blue, yellow, and purple balls, respectively

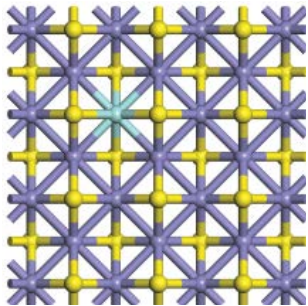
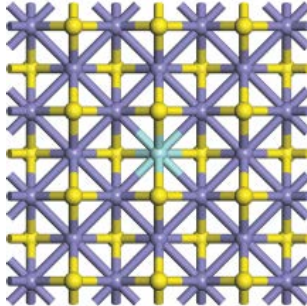
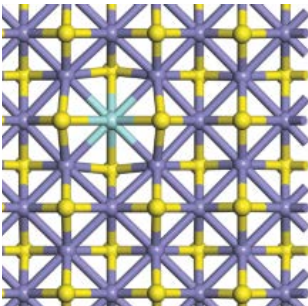
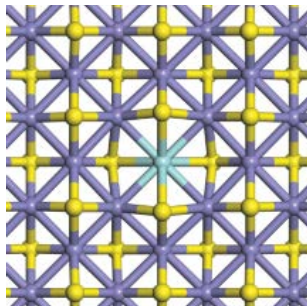
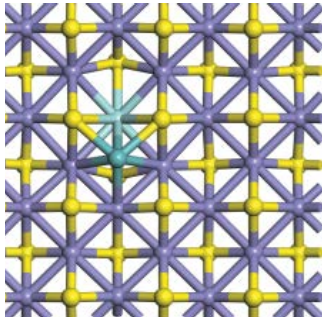
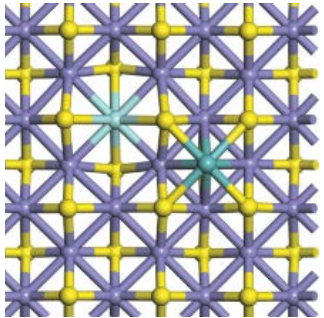
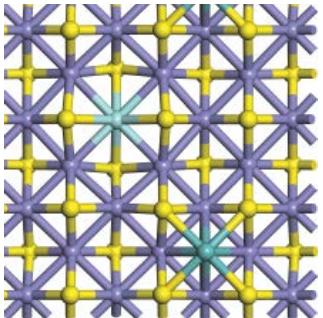
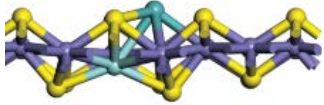
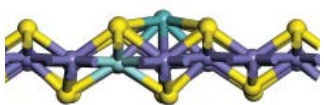
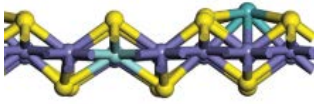
Sites	Model 1	Model 2
Before optimization		
After optimization		
Zr-S shortest (Å)	2.47	2.45
E_{ads} (Zr/FeS) (eV)	-2.95	-2.89

Table S3

Optimization results of Mo on different adsorption sites of Zr/FeS (001). The purple, yellow, light green, and green balls represent iron, sulfur, zirconium, and molybdenum atoms, respectively

Sites	Absorb 1	Absorb 2	Absorb 3
Top view			
Side view			
$D_{\text{Mo-Zr}}$ (Å)	2.71	4.50	6.79
E_{ads} Mo@Zr/FeS(001) (eV)	-7.61	-7.44	-7.19

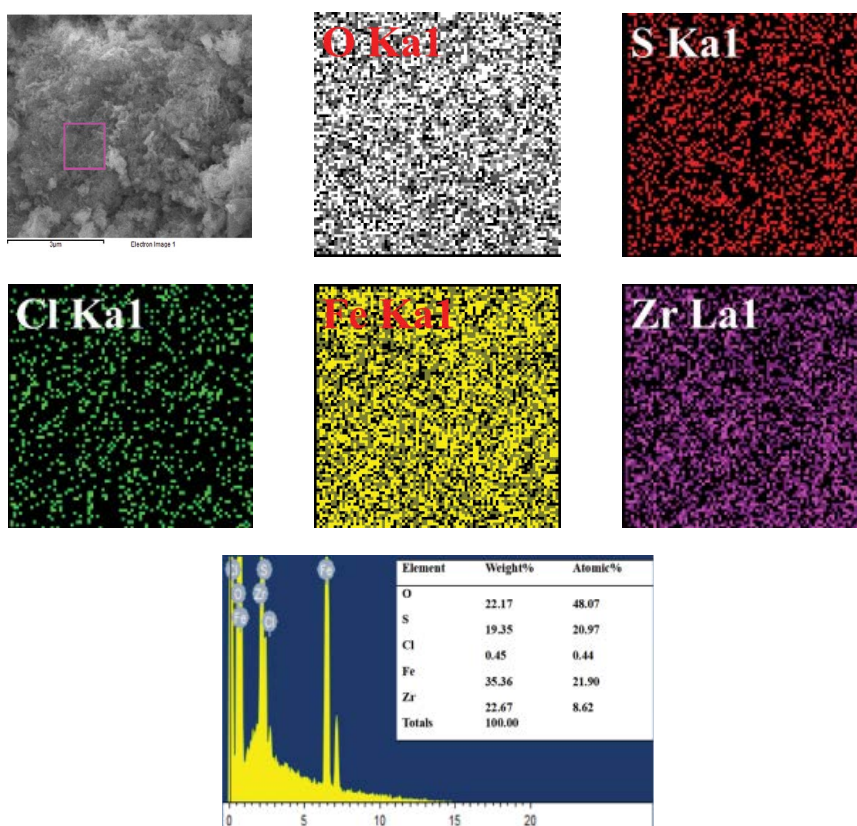


Fig. S1. Scanning electron microscopy mapping images of Zr-FeS, the order of the elements is: O, S, Cl, Fe, Zr, and EDS images of Zr-FeS.

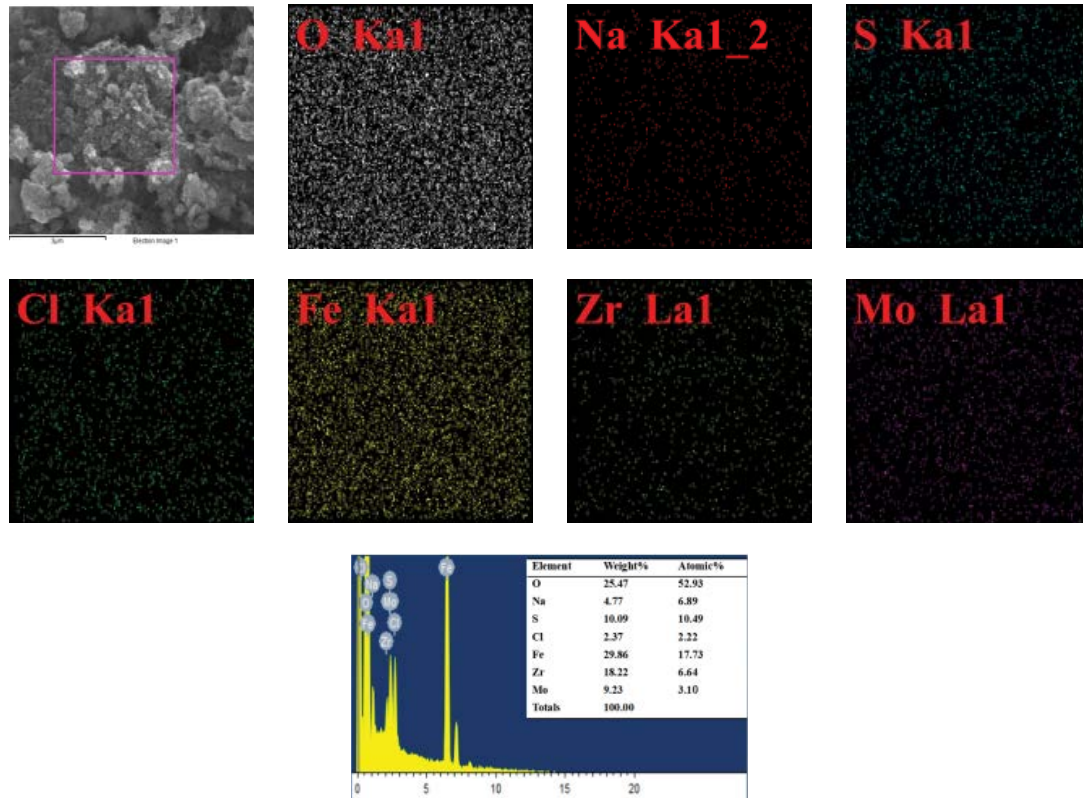


Fig. S2. Scanning electron microscopy mapping images of Zr-FeS-Mo, the order of the elements is: O, Na, Cl, Fe, Mo, S, Zr, and EDS images of Zr-FeS-Mo.

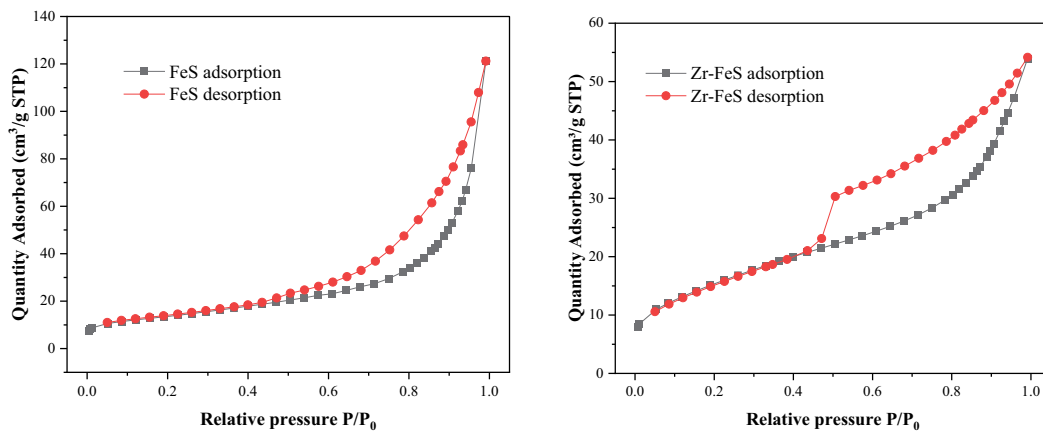


Fig. S3. Nitrogen adsorption–desorption isotherms of (a) FeS and (b) Zr-FeS.

Reference

[S1] P.N. Fotsing, E.D. Woumfo, S. Mezghich, M. Mignot, N. Mofaddel, F.L. Derf, J. Vieillard, Surface modification of biomaterials based on cocoa shell with improved nitrate and Cr(VI) removal, RSC Adv., 10 (2020) 20009–20019.